Method of separation of vibrational motions for applications involving wetting, superhydrophobicity, and microparticle extraction

Md Syam Hasan and Michael Nosonovsky*
Department of Mechanical Engineering, University of Wisconsin-Milwaukee, 3200 North Cramer Street, Milwaukee, Wisconsin 53211, USA

(Received 1 November 2019; accepted 31 March 2020; published 4 May 2020; corrected 20 August 2020)

Nonlinear small-amplitude high-frequency vibrations affect mechanical systems leading to such effects as the stabilization of an inverted pendulum on a vibrating foundation and size separation of particles of a granular material. These effects can be studied using the mathematical technique called "the method of separation of fast and slow motions." When applied to fluid mechanics applications, the method predicts various unusual effects including jamming holes in a vibrating tank with liquid, vibrational propulsion, and multiphase flow separation. Many of these effects have been confirmed experimentally. Here we discuss the possibility of similar microfluidic effects in applications where capillary forces dominate over viscosity and inertia, such as vibrational aeration, vibration-induced superhydrophobicity (the elimination of the contact angle hysteresis), and vibrational two-phase flow separation for microparticle extraction.

DOI: 10.1103/PhysRevFluids.5.054201

I. INTRODUCTION

Micro- and nanofluidics is a relatively new and rapidly growing area of research, which is often combined with microelectromechanical systems (MEMS) and lab-on-a-chip, novel technologies of miniaturized electromechanical systems. In lab-on-a-chip devices, carrier liquids can circulate through arrays of microchannels forming a complex microfluidic network on a single chip of a few square centimeters. At microscopic and nanoscopic levels, liquid behavior and flow property vary significantly from those at a macroscopic level [1]. In macroscale hydraulics, pressure and gravity force dominate in fluid dynamics over capillary forces, van der Waals forces, and surface tension. However, at the microscale, this consideration is reversed. As the surface-to-volume ratios increase with miniaturization, fluid mechanics of microdroplets is dominated by the capillary forces, adhesion, and surface tension, while volume forces such as gravity and pressure forces become insignificant. As a result, wetting, capillarity, and surface phenomena including superhydrophobicity become crucial for designing and manufacturing the microdevices.

Macroscale fluid flow combined with high-frequency vibrations creates effective acoustic forces, which can be determined using the mathematical methods of separation of motions and averaging the effect of small-amplitude vibrations. Due to various hysteresis effects, averaging by the period of vibrations yields a nonzero contribution to the effective acoustic force. Hysteresis of the fluid flow is found in macroscale applications; however, it is even more pronounced with the capillary phenomena dominating at the microscale.

The contact angle (CA) between a liquid and a solid surface is the conventional way of quantitating the wettability of the surface by the liquid. A surface that is wetted by water producing

*Corresponding author: nosonovs@uwm.edu

 ©2020 American Physical Society

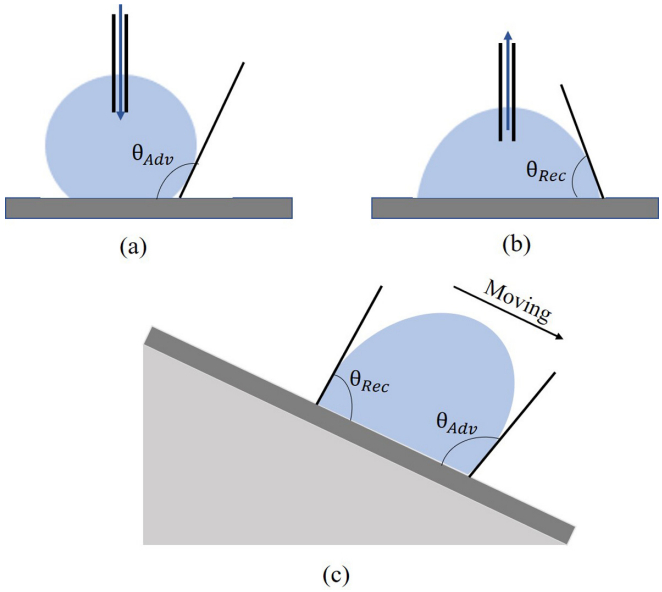

FIG. 1. (a), (b) Schematic of the sessile-drop method to measure contact angle hysteresis (CAH). (c) Schematic of advancing and receding contact angles on the tilting plate.

a CA less than 90° is known as a hydrophilic surface. As a result of its low surface energy, a hydrophobic surface reduces the contact area between the solid surface and a water droplet by producing a higher CA of more than 90°. CAs higher than 150° are typical for superhydrophobic surfaces, which have further reduced contact area between the solid surface and the liquid droplet.

In many cases, the measured value of the CA depends on whether liquid advances or recedes. The advancing CA (θ_{Adv}) is usually higher than the receding CA (θ_{Rec}) corresponding to the maximum and the minimum values of the CA on a solid substrate when a liquid droplet is placed on it. Figures 1(a) and 1(b) show the sessile drop method of measuring θ_{Adv} and θ_{Rec}. In Fig. 1(a) the volume of the sessile droplet is gradually increased by adding liquid by a syringe. The maximum possible contact angle is known as θ_{Adv} [2]. In Fig. 1(b), θ_{Rec} is measured by reducing the volume from the droplet using the syringe until dewetting occurs. Figure 1(c) shows the method of measuring θ_{Adv} and θ_{Rec} using a tilting plate. A sessile drop is placed on the plate and it is slowly tilted until the droplet starts moving in the downhill direction. Just before the droplet starts moving, the downhill CA and the uphill CA are referred to as the θ_{Adv} and θ_{Rec}, respectively.

Contact angle hysteresis (CAH) is defined as the difference between the advancing and the receding contact angles. The contact angle and contact angle hysteresis are two quantitative measures of adhesion between water and a solid surface [3]. Water repellent surfaces, such as superhydrophobic surfaces are characterized by low values of CAH.

Chemical and topographical heterogeneity (roughness) of the surface is considered as the major reason behind CAH [4]. CAH resists the sliding or rolling of the water droplet on an inclined surface by pinning the contact line (CL) in metastable positions. The contact line is the line where the liquid, solid, and vapor phases meet. The effects of micro- and macroscale roughness on surface wetting properties and the process of the manufacturing of superhydrophobic and hydrophilic surfaces have been studied extensively [5–9]. The reduction of CAH by minimizing the liquid-solid contact of the solid substrate and the liquid droplet is a requirement in many engineering applications. Vibration can be used in modifying several wetting properties such as the CAH.

The effects of vibration in fluid dynamics have been studied at the macroscale [10–12]. However, there has been very little of such research at the microscale. Vibration and acoustics

forces become powerful tools for handling and characterizing fluids and particles in microscale, for example, to study capillary systems and predict the flow characteristics of lab-in-a-chip and microelectromechanical systems. In this study, we will use the method of separation of motions to investigate the effect of vibration on the capillarity and wetting properties, such as CAH and superhydrophobicity and microparticle separation from fluid flow in piezo tube resonators.

II. MATHEMATICAL MODEL OF SEPARATION OF MOTIONS

In this section, we introduce the mathematical method of separation of slow and fast motions. This method is particularly powerful when applied to the study of the motion combined with high-frequency small-amplitude vibrations. When a system is under vibration, the resulting motion can be expressed as a sum of two components—the "slow" overall (e.g., macroscale) motion and the "fast" low amplitude (e.g., microscale) vibrational component imposed over the slow motion [13–16].

$$m\ddot{x} = -\frac{d\Pi}{dx} + f\cos t, \tag{1}$$

where $\Pi(x)$ is the potential energy of the system, m is the mass, and ω is the frequency of the vibration. $F = -\frac{d\Pi}{dx}$ is the slow force and $f\cos\omega t$ is the fast oscillating force having amplitude f. Kapitza suggested that using the theory of separation of motions, small, fast vibrations can be replaced by an effective force [14]. This effect can be applied to model numerous engineering systems.

Landau and Lifshitz suggested the solution as a summation of the slow and fast oscillating motions [16]:

$$x(t) = X(t) + \xi(t). \tag{2}$$

$\xi(t)$ corresponds to the small oscillation and the mean value of the function is zero over the period $\frac{2\pi}{\omega}$:

$$\langle\xi(t)\rangle = \frac{\omega}{2\pi}\int_0^{\frac{2\pi}{\omega}} \xi(t)dt = 0. \tag{3}$$

$X(t)$ changes slightly over the period and describes the "smooth" motion of the particle averaged over the rapid oscillation. The equation of the motion can be given as

$$m\ddot{X} = -\frac{d\Pi_{\text{eff}}}{dX}, \tag{4}$$

where $d\Pi_{\text{eff}}$ is the effective potential energy:

$$\Pi_{\text{eff}} = \Pi + \frac{m}{2}\langle\dot{\xi}^2\rangle = \Pi + \frac{f^2}{2m^2}. \tag{5}$$

The additional term in the potential energy appears because of the small-amplitude fast vibration ξ averaged over the period $\frac{2\pi}{\omega}$. The effect of the fast small-amplitude vibrations can also be perceived as an effect of some new effective force.

This effective vibrational force may have a stabilizing effect. It can also be described in terms of the change in effective potential energy. If the additional effective force for the system is denoted as V, its equation can be written as

$$V = -\frac{\partial}{\partial X}\left[\frac{1}{2m^2}\frac{\omega}{2\pi}\int_0^{\frac{2\pi}{\omega}} (f\cos t)^2 dt\right] = -\frac{\partial}{\partial X}\left(\frac{f^2}{4m^2}\right). \tag{6}$$

Blekhman suggested an interpretation of this fictitious effective force, which is in a sense similar to the inertia force, also fictitious and observed in noninertial frames in Ref. [17]. According to his interpretation, the vibrational effective force is detected by an observer who does not observe the

small-amplitude vibration for one or another reason, such as the stroboscopic effect (if the light flashes with the same frequency as the vibration) or just due to the amplitude being smaller than the optical spatial resolution. Such observer interprets the effect of the fast vibration as a result of action of a certain slow force. Vibrational closure of holes and pores, synchronization of rotating machinery, formation of bubbles for chemical processes, separation of granular material, and many more engineering phenomena can be explained by this theory. In certain cases, the vibrational effect is similar to phase transition, i.e., an effective "freezing" of liquid or "melting" of a granular material and size separation of particles of a granular material.

Below we will discuss several applications of the separation of motions to the microfluidic problems including the vibrational closure of holes, air bubble injection, vibrational elimination of contact angle hysteresis, and multiphase flow separation.

III. VIBRATIONAL CLOSURE OF HOLES IN A LIQUID-FILLED TANK AND TRANSPORT OF BUBBLES

In this section, we discuss the possibility of effectively closing a hole in a macroscopic tank with liquid on a vibrating foundation as a result of vibration. Due to the asymmetry of water flow in the opposite directions, small-amplitude high-frequency vibrations prevent water penetration through the hole. Such asymmetry or hysteresis is well known for small-scale systems where surface tension forces dominate over volume forces. This is contact angle hysteresis or adhesion hysteresis during the wetting-dewetting cycle. However, hysteresis exists even for large systems where hydrodynamic forces dominate over the interfacial phenomena. This is due to various nonlinear effects, in particular, the asymmetry of the coefficient of discharge during liquid advance and recess.

A. Effective freezing or preventing liquid flow through a hole

If a uniform circular hole is introduced at the bottom of a fluid-filled tank, the fluid will leak out through the hole as a consequence of the hydrostatic pressure difference inside and outside the tank. When a high-frequency vibration is imposed on the liquid-filled tank, the draining out of the fluid can be slowed down or even stopped. In this case, the hydrostatic pressure difference causing the discharge of the fluid through the hole will be balanced by the effective counterpressure appearing due to vibration.

Following the derivation by [17], let us consider a tank (Fig. 2) containing a certain fluid 1 (e.g., water) of density ρ_1, and outside there is another fluid 2 (e.g., air) of density ρ_2. The height of the

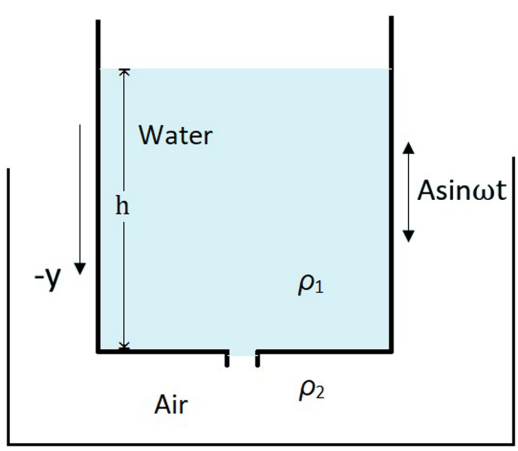

FIG. 2. A vibrating tank with a hole, containing the fluid.

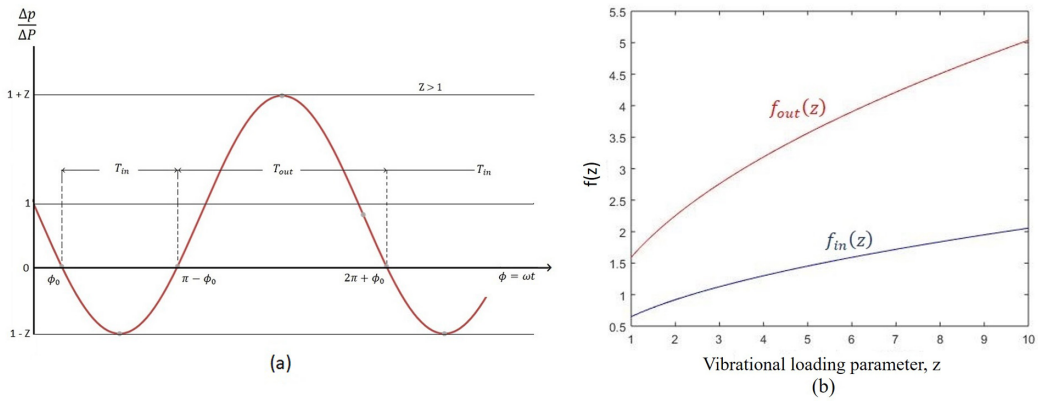

FIG. 3. (a) Dimensionless pressure difference ($\frac{\Delta p}{\Delta P}$) versus time leading to the inflow of air and outflow of water. (b) Plots of the functions $f_{\text{out}}(z)$ and $f_{\text{in}}(z)$ versus vibrational loading parameter, z.

liquid column is h, and there is a hole at the bottom of the tank. The static pressure difference at the hole is $\Delta P = P_1 - P_2 > 0$, where P_1 and P_2 are the pressures inside and outside of the tank. This static pressure difference can be expressed as $\Delta P = (\rho_1 - \rho_2)hg$, where g is the gravitational acceleration. The equation of volume flow rate of water through a hole is given by

$$Q = C_{\text{dout}} S \sqrt{\frac{2\Delta P}{\rho_1}}. \tag{7}$$

Here C_{dout} is the coefficient of discharge (COD) of water and S is the cross-sectional area of the hole.

The COD is the ratio of the amount of actual fluid discharge to the amount theoretically possible at that pressure [18]. Viscous friction of the fluid, boundary slip, non-Newtonian properties, and other factors deviating fluid properties from those of an ideal liquid, as well as the asymmetry in the shape of the hole, cause the difference in theoretical and actual discharge of a liquid through an opening. The COD may depend on the dimensionless Reynolds number (i.e., the ratio of inertial force to viscous force) of the flow, geometrical configuration of the opening, temperature, and on some of the factors. Note that the value of the COD for water advancing into a pipe or through a hole may be different from that of receding water. This is the key property leading to the asymmetry.

When the vibration in the vertical direction is introduced, the tank oscillates as $y = A \sin \omega t$, where A is the amplitude and ω is the frequency of the vibration. The acceleration of the tank in the vertical direction is $\ddot{y}$. In a noninertial coordinate system, the force of inertia acts, and the effective value of the gravity constant becomes $(g - \ddot{y})$. The equation of the dynamic pressure difference, Δp (when vibration is introduced) is

$$\Delta p = \rho_1 h(g - \ddot{y}) = \Delta P - \rho_1 h \ddot{y} = \Delta P(1 - z \sin \phi). \tag{8}$$

Here, $\phi = \omega t$ is the phase angle and z is the vibrational loading parameter, which is the ratio of the amplitude of the dynamic pressure to the static pressure difference.

$$z = \frac{\rho_1 h A \omega^2|}{\Delta P}. \tag{9}$$

For a high frequency ($z > 1$), in a complete vibration cycle, both flowing in of air into the tank and flowing out of water from the tank occur, although the time interval for the outflow, T_{out}, is greater than that of the inflow, T_{in}, due to gravity, as shown in Fig. 3(a). This is because $\frac{\Delta p}{\Delta P}$ is positive only during $\pi - \phi_0 < \phi < 2\pi + \phi_0$ (here, $\phi_0 = \sin^{-1} \frac{1}{z}$ is the initial phase angle).

Even though $T_{\text{out}} > T_{\text{in}}$, the difference in COD for the flow in both directions can result in effective stopping of the flow. The volume flow rates of water flowing out from the vibrating tank and of air flowing in are given by [19]

$$Q_{\text{out}}^{T} = \frac{\omega}{2\pi} C_{\text{dout}} S \sqrt{\frac{2\Delta P}{\rho_1}} \int_{\frac{\pi-\phi_0}{\omega}}^{\frac{2\pi+\phi_0}{\omega}} \sqrt{1 - z\sin\omega t}\, dt = \frac{1}{2\pi} C_{\text{dout}} S \sqrt{\frac{2\Delta P}{\rho_1}}\, f_{\text{out}}(z), \tag{10}$$

$$Q_{\text{in}}^{T} = -\frac{\omega}{2\pi} C_{\text{din}} S \sqrt{\frac{2\Delta P}{\rho_2}} \int_{\frac{\phi_0}{\omega}}^{\frac{\pi-\phi_0}{\omega}} \sqrt{z\sin\omega t - 1}\, dt = \frac{1}{2\pi} C_{\text{din}} S \sqrt{\frac{2\Delta P}{\rho_2}}\, f_{\text{in}}(z), \tag{11}$$

where C_{dout} and C_{din} are the coefficients of discharge of water flowing out and air flowing into through the hole, $f_{\text{out}}(z) = \omega \int_{\frac{\pi-\phi_0}{\omega}}^{\frac{2\pi+\phi_0}{\omega}} \sqrt{1 - z\sin\omega t}\, dt$ and $f_{\text{in}}(z) = -\omega \int_{\frac{\phi_0}{\omega}}^{\frac{\pi-\phi_0}{\omega}} \sqrt{z\sin\omega t - 1}\, dt$.

The total average volume flow rate per complete cycle of the vibration is

$$Q^{T} = Q_{\text{out}}^{T} + Q_{\text{in}}^{T} = \frac{S\sqrt{\frac{2\Delta P}{\rho}}}{2\pi}[C_{\text{out}} f_{\text{out}}(z) - C_{\text{in}} f_{\text{in}}(z)]. \tag{12}$$

For the vibrational closure of the tank, the total average volume flow rate per complete cycle of the vibration needs to be zero, $C_{\text{dout}} f_{\text{out}}(z) = C_{\text{din}} f_{\text{in}}(z)$.

Following the calculations in [19], the integrands can be presented as

$$f(z) = 4\sqrt{2z}[E(k) - (1 - k^2)K(k)], \tag{13}$$

where $k = \sqrt{\frac{z\pm 1}{2z}}$ (the plus and minus signs correspond to f_{out} and f_{in}) and K and E are the complete elliptical integral of first and second kind, respectively. The plots of $f_{\text{out}}(z)$ and $f_{\text{in}}(z)$ versus z are shown in Fig. 3(b) based on a MATLAB calculation for $1 \leqslant z \leqslant 10$. From the plot, $f_{\text{out}}(z) > f_{\text{in}}(z)$ for any value of $z \geqslant 1$. Moreover, the value of $f_{\text{out}}(z)$ becomes significantly greater than $f_{\text{in}}(z)$ for higher values of z.

The value of the COD of water (flowing out from the vibrating tank) and the air (flowing in the tank) is the most crucial factor for achieving vibrational closure of the vibrating tank. For water flowing out from the tank, the frictional head loss is significant. The head loss represents the energy used in overcoming viscous friction caused by the walls of the pipe, tank and other equipment. The equation of head loss is given by

$$h_f = \frac{32\mu L V}{\rho g d^2}, \tag{14}$$

where μ is the dynamic viscosity of the fluid, L is the length of the pipe or tank, d is the hydrodynamic diameter of the tank, and ρ is the density of the fluid. For the water flowing out from the vibrating tank, the hydraulic diameter of the tank is a finite number; as a result there will be a finite value of the head loss. Because of the head loss, the actual discharge of water will be different from the theoretical discharge, and the coefficient of discharge $C_{\text{dout}} < 1$ will be significantly smaller than unity.

On the other hand, air entering the vibrating tank experiences a negligible frictional head loss. Air will enter the vibrating vessel from the environment. In this case, the hydraulic diameter is assumed to be a very large number. As a result, the frictional head loss is negligible, and the actual discharge is similar to the theoretical discharge. So, the coefficient of discharge (C_{din}) is very close to 1. Also, the coefficient of discharge of the water flowing out can be reduced significantly by changing the circular hole to a conic shape narrowing outside. Due to the higher value of the coefficient of discharge of air entering the vibrating tank than that of water flowing out from it, the vibrational closure of the tank is achieved at $C_{\text{dout}} f_{\text{out}}(z) = C_{\text{din}} f_{\text{in}}(z)$.

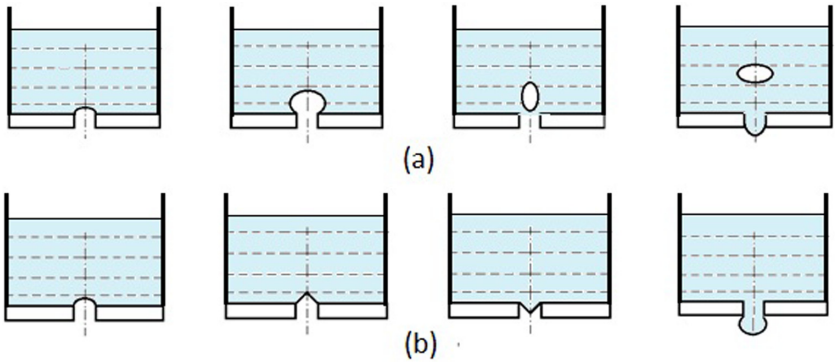

FIG. 4. The sequential steps of the air injection through the hole. The cases when the volume of the gas that enters the tank is (a) sufficient to form bubbles or (b) insufficient, so that the air injection does not take place (based on [17]).

B. Air bubbles injection into a vibrating tank

The formation of air bubbles is a complex mechanism where numerous variables govern its creation. In classical fluid mechanics, the volume flow rate of air and the orifice geometry are considered as the most dominating influences on bubble formation. In our study, we have analyzed the mechanism of bubble formation from a different point of view using small, fast vibration. For the vibrating tank, the air can flow into the tank if $\frac{C_{\text{dout}}}{C_{\text{din}}} < \frac{f_{\text{in}}(z)}{f_{\text{out}}(z)}$. Figure 4 shows the sequential steps of a successful air injection event in a vibrating tank and an unsuccessful one.

For the formation of bubbles, the volume of the gas entering the vibrating tank through a hole with the diameter d should satisfy

$$V = \frac{2\pi}{\omega} Q_{\text{in}}^{T} = \frac{C_{\text{din}} S}{\omega} \sqrt{2gh \frac{\rho_{\text{out}}}{\rho_{\text{in}}}}\, f_{\text{in}}(z) > \frac{\pi d^3}{6}. \tag{15}$$

Now assuming $V = \frac{\pi d^3}{6}$ we can find the critical height, h_{cr} of the liquid column. For any height of the liquid column larger than h_{cr}, air injection in the vibrating tank takes place.

$$h_{cr} = \frac{2}{9} \frac{\rho_2}{\rho_1} \frac{d^2 \omega^2}{C_{\text{din}}^2 f_{\text{in}}^2(z) g}. \tag{16}$$

The ratio of the densities of air and water ($\frac{\rho_2}{\rho_1}$) is a small number. When the vibration is intensive enough [$z > 3$ and $f_{\text{in}}(z)$ is large], the value of the critical height, h_{cr}, of the water column is quite small. However, it can be substantial when the vibration is not intensive [$z < 1.5$ and $f_{\text{in}}(z)$ is small] [19].

Experimental verification of the vibrational air injection has been reported by Blekhman and co-workers [17,19] in their experiments with a vibrating glass vessel (300 mm height, 58 mm diameter) with a hole in the bottom. A certain amount of water was kept in the vessel and the vessel was subjected to a vertical vibration where the amplitude and frequency could be changed within certain limits. Air was sucked in the form of bubbles and the process was monitored in stroboscopic light. The diameter of the hole, d, amplitude of the vibration, A, and the height of the liquid column, h, were kept constant ($d = 2.6$ mm, $A = 2.5$ mm, $h = 200$ mm). The volume flow rate of water flowing out from the vibrating tank, Q_{out}^{T}, and the volume flow rate of the air flowing in the vibrating tank, Q_{in}^{T}, were measured with varying the vibrational loading parameter, z. Experimentally it was observed that, with the increase of the value z from $z = 1$, Q_{out}^{T} first diminished and then started to grow with increased z. This result supports our theory presented earlier. From Eq. (10), it is understood that with the growing value of z, Q_{out}^{T} should decrease. But, as the vibration gets more

intense, the pressure difference at the hole increases and becomes dominant in Eq. (10) to increase the value of Q^T_{out} [17].

On the other hand, Q^T_{in} increased monotonously in the experimental demonstration with the increase of the vibrational loading parameter, z. This experimental demonstration thus corroborates the theoretical expression developed earlier. Theoretically, we predicted possible bubble formation for any value of $z > 1$. But experimentally, a considerable amount of bubble injection was first noticed only after the value of the loading parameter reached $z = 2.5$. This phenomenon can be explained by the effect of the surface tension at the time of bubble formation [19].

Another important area where vibrational injection of air bubbles can be used is vibration-induced aeration [20]. Aeration is the process by which air is dissolved in or circulated through a liquid. Various types of aeration are often used; however, water aeration is typically achieved by passing water through air or air through water with the use of porous surfaces. Bubble diffusers producing small air bubbles are used for wastewater treatment. As surface-to-volume area changes proportionally to the bubble size, small bubbles increase the rate of gas transfer due to the higher contact surface area. The pores which these bubbles pass through are generally micrometer size. Vibrating membrane aeration can be used utilizing the air injection effect.

IV. VIBRATION-INDUCED SUPERHYDROPHOBICITY

In this section, we will discuss the effect of vibration on the wetting of solid surfaces, which can dramatically change wetting properties leading to the vibration-induced superhydrophobicity [21,22].

Dong *et al.* [23], and Noblin *et al.* [24], in their studies, analyzed the impact of a droplet's own natural frequency and resonance modes of the vibrating water drop on its locomotion. In their recent study, Mettu and Chaudhury [25] represented a systematic analysis of the effect of asymmetric vibration on the motion of liquid drops and overcoming CAH.

To estimate the importance of the resonance effect at a given frequency, let us calculate Rayleigh's natural frequencies of a water droplet with the radius R undergoing a capillary vibration given by $\omega_n = \sqrt{\frac{n(n-1)(n+2)\gamma_{lv}}{\rho R^3}}$, where $n = 2, 3, 4\cdots$, $\gamma_{lv} = 0.072\,\text{N/m}$, and $\rho = 1000\ \text{kg/m}^3$ are the surface tension and density of water. For $n = 2$ and $R = 0.5$ mm the fundamental natural frequency is $\omega_n = 2150\,\text{rad/s}$. In our study, we concentrate the effect of small, fast vibrations on CAH for lower typical frequencies; therefore, we do not discuss the resonance effects. These effects can become significant under certain circumstances.

Superhydrophobicity is the extreme water repellence of a solid surface, which is usually achieved by a combination of the surface roughness and a low surface energy coating [26]. Quantitatively, superhydrophobicity is characterized by high values of the water CA $>150°$ and low hysteresis of the CA (typically, $<10°$).

The equilibrium value of the most stable CA, θ_0, is given by the Young equation [27],

$$\cos\theta_0 = \frac{\gamma_{sv} - \gamma_{sl}}{\gamma_{lv}}, \tag{17}$$

where γ_{sv}, γ_{lv}, and γ_{sl} are the surface tension forces (or interfacial energies) of the solid-vapor, the liquid-vapor, and the solid-liquid interfaces, respectively, acting on the contact line. The Young equation is often interpreted as the equilibrium condition of the three surface tensions, when only the horizontal (parallel to the solid surface) components of the surface tension forces, $\gamma_{lv}\cos\theta_0 - \gamma_{sv} + \gamma_{sl} = 0$ are considered [Fig. 5(a)]. It is assumed that the vertical component of the surface tension force is balanced by the reaction of the substrate, $N_0 = \gamma_l \sin\theta_0$. Hysteresis of the CA corresponds to the rotation of the vector γ_l for a certain angle, as the value of γ_{sl} changes during wetting and dewetting due to adhesion hysteresis [28,29].

Let us now consider a small-amplitude fast vibration of the solid substrate in the vertical direction $y = A\sin\omega t$, where A is the amplitude and ω is the frequency of the vibration. Due to

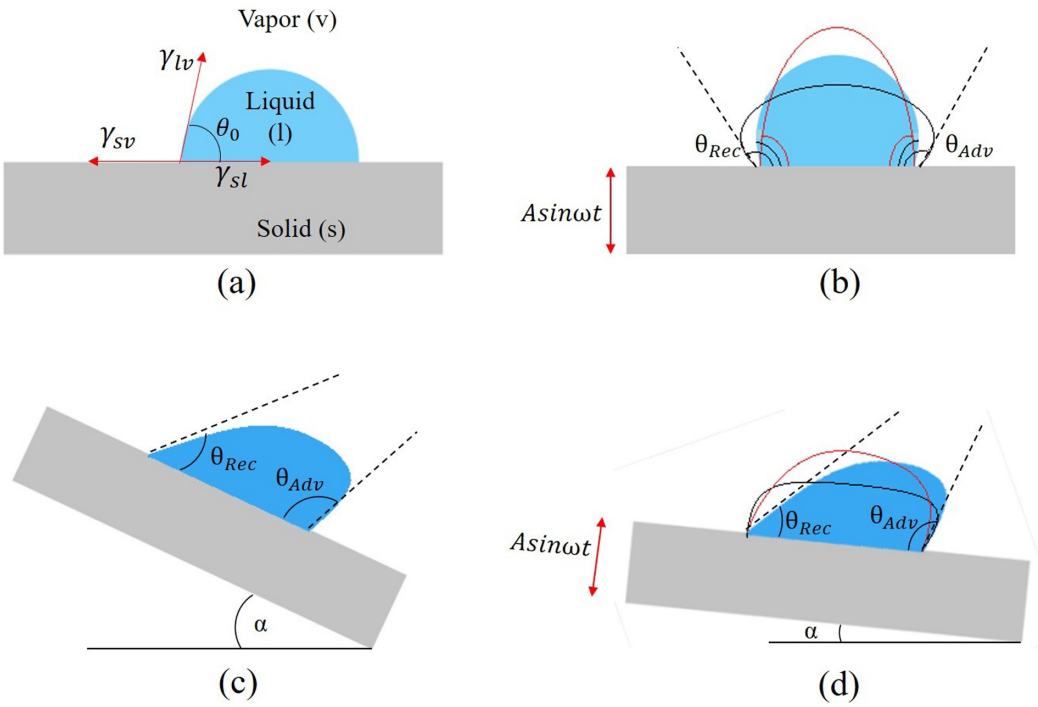

FIG. 5. (a) The equilibrium of forces at the three-phase line for a water droplet placed on a chemically homogeneous smooth solid substrate. (b) Mode shapes of the water droplet due to vibration. (c) A droplet is placed on a tilted surface with a tilt angle α and the advancing and receding CA. (d) The reduction of tilt angle required for initiating droplet motion when the vibration is introduced to the solid substrate.

the vibration, an additional inertia force, $\gamma_{\text{in}}(t)$, acts upon the contact line in the vertical direction, so that the reaction of the substrate is $N = N_0 + \gamma_{\text{in}}(t)$, which affects the equilibrium of forces at the three-phase line. This inertia force is proportional to the acceleration of the substrate; i.e., $\gamma_{\text{in}} = -A\omega^2 \sin \omega t$. As a result, the equilibrium of the vertical components of the surface tension force is expressed as $N_0 + \gamma_{\text{in}}(t) = \gamma_{lv} \sin\theta$ or

$$\gamma_{lv} \sin\theta = \gamma_{lv} \sin\theta_0 - A\omega^2 \sin \omega t. \tag{18}$$

In other words, the value of the CA may change periodically, as shown in Fig. 5(b), between

$$\sin\theta = \sin\theta_0 \pm A\omega^2/\gamma_{lv} \tag{19}$$

When the maximum value of the CA exceeds that of the advancing CA, $\sin\theta_0 + A\omega^2/\gamma_{lv} \geqslant \sin\theta_{\text{Adv}}$, the pinning cannot hold the three-phase line and it advances. This inertial effect can be interpreted as an equivalent reduction of the observed value of the advancing CA. Similarly, the observed value of the receding CA increases. Consequently, observed CAH (which is defined as the difference between the θ_{Adv} and θ_{Rec}) is reduced for the value dependent on $2A\omega^2/\gamma_{lv}$. When the vibration is intense enough, so that $2A\omega^2/\gamma_{lv} \geqslant |\sin\theta_{\text{Adv}} - \sin\theta_{\text{Rec}}|$, it is expected that CAH is significantly reduced.

In Fig. 5(c), a droplet is placed on a tilted surface with a critical tilt angle α, and it sticks to the surface instead of flowing along the tilted surface. A small increase of the tilt angle α will initiate the sliding of the water droplet along the surface. The resistance against the droplet's sliding along the solid surface due to the pinning of the three-phase contact line (CL) in metastable positions [30] is responsible for the CAH phenomenon. When a high-frequency small-amplitude vibration

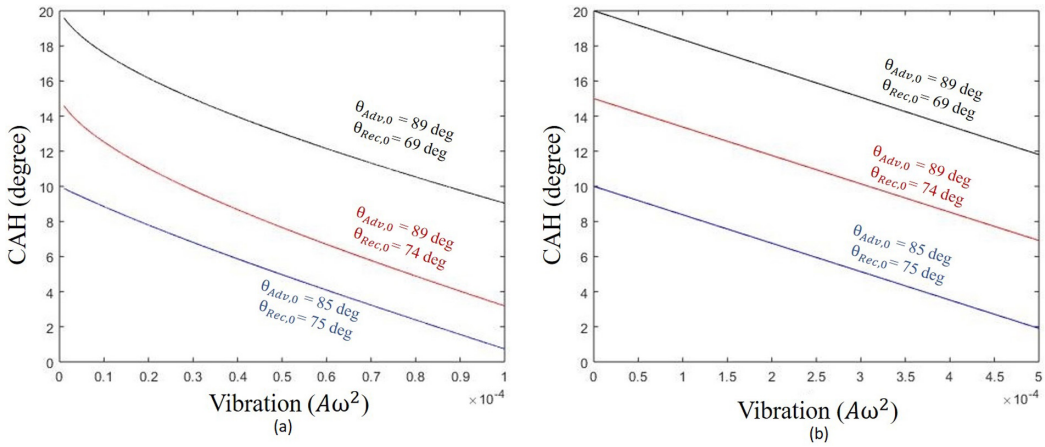

FIG. 6. Relation of CAH and vibration level ($A\omega^2$) when the solid substrates are subject to (a) vertical and (b) horizontal vibrations.

is introduced to the solid substrate in the vertical direction, the resulting inertial force γ_{in} on the droplet can trigger the droplet's motion along the tilted surface effectively decreasing the observed CAH as shown in Fig. 5(d).

Let us consider a case where water droplets are placed on three different solid substrates having CAH values of 20° ($\theta_{\text{Adv}} = 89°$, $\theta_{\text{Rec}} = 69°$), 15° ($\theta_{\text{Adv}} = 89°$, $\theta_{\text{Rec}} = 74°$) and 10° ($\theta_{\text{Adv}} = 85°$, $\theta_{\text{Rec}} = 75°$). When the vibration is applied to the solid substrates in the vertical direction, the observed minimum and maximum values of the advancing and receding CAs were calculated using the following two equations ($\gamma_{lv} = 72.8 \times 10^{-3}$ N/m is water surface tension at 20 °C).

$$\theta_{\text{Adv}} = \sin^{-1}(\sin\theta_{\text{Adv0}} - A\omega^2/\gamma_{lv}), \tag{20}$$

$$\theta_{\text{Rec}} = \sin^{-1}(\sin\theta_{\text{Rec,0}} + A\omega^2/\gamma_{lv}). \tag{21}$$

The results for CAH are presented in Fig. 6(a) for the vertical vibration level ($A\omega^2$) changing in the range of 10^{-6} N/m to 10^{-4} N/m. It is seen from the graph that at a small vibration level ($A\omega^2 \approx 0$ N/m), the CAH is almost equal to the actual value. Then the CAH was reduced dramatically with the increase of the vibration level. In this study, $A\omega^2 = 10^{-4}$ N/m was considered as the maximum vibration level and at that point the CAH hit the minimum value for each substrate.

As the second case, let us now consider a small-amplitude fast vibration of the solid substrate in the horizontal direction $y = A\sin\omega t$, where A is the amplitude and ω is the frequency of the vibration. Due to the vibration, an additional inertia force, $\gamma_{\text{in}}(t)$, acts upon the contact line in the horizontal direction which affects the equilibrium of forces at the three-phase line. The force balance in the horizontal direction becomes $\gamma_{lv}\cos\theta - \gamma_{sv} + \gamma_{sl} + \gamma_{\text{in}} = 0$. The inertia force is proportional to the acceleration of the substrate; i.e., $\gamma_{\text{in}} = -A\omega^2\sin\omega t$. As a result, the equilibrium of the horizontal components of the surface tension force is expressed as $\gamma_{lv}\cos\theta - \gamma_{sv} + \gamma_{sl} - A\omega^2\sin\omega t = 0$ or $\cos\theta = \frac{\gamma_{sv}-\gamma_{sl}}{\gamma_{lv}} + \frac{A\omega^2\sin\omega t}{\gamma_{lv}}$.

In other words, the value of the CA may change periodically, between

$$\cos\theta = \cos\theta_0 \pm \frac{A\omega^2}{\gamma_{lv}}. \tag{22}$$

When the maximum value of the CA exceeds that of the advancing CA (i.e., $\cos\theta_0 \pm \frac{A\omega^2}{\gamma_{lv}} \geqslant \cos\theta_{\text{Adv}}$) the pinning cannot hold the three-phase line and the water droplet advances. This inertial effect can be interpreted as an equivalent reduction of the observed value of the advancing CA.

Similarly, the observed value of the receding CA increases. Consequently, observed CAH is reduced for the value dependent on $2A\omega^2/\gamma_{lv}$. When the vibration is intense enough, so that $2A\omega^2/\gamma_{lv} \geqslant |\cos\theta_{\mathrm{Adv}} - \cos\theta_{\mathrm{Rec}}|$, it is expected that the water droplet will overcome the resistance against the CL motion, and the CAH is almost completely eliminated [22]. Note that CAH is a fundamental property inherent for any real surface [29], so, as opposed to the ideal case, it is unlikely that CAH can be eliminated completely on a real surface, but rather significantly reduced. Consequently, the surface exhibits hydrophobic and superhydrophobic behaviors and water droplets placed on it can move by sliding, rolling, or by a combination of these two motions. Note that the apparent reduction of CAH is due to vibrations helping to overcome CAH more readily; therefore, we are dealing here with an effective (apparent) reduction of CAH, similarly to the effects considered in the preceding sections.

Let us consider that water droplets are placed on three different solid substrates having CAH values of 20 ($\theta_{\mathrm{Adv}} = 89$, $\theta_{\mathrm{Rec}} = 69^\circ$), 15 ($\theta_{\mathrm{Adv}} = 89$, $\theta_{\mathrm{Rec}} = 74^\circ$), and 10 ($\theta_{\mathrm{Adv}} = 85$, $\theta_{\mathrm{Rec}} = 75^\circ$). When the vibration is introduced to the solid substrates in the horizontal direction, the observed minimum and maximum values of the θ_{Rec} and of the θ_{Adv} were calculated using the following two equations. γ_{lv} is the surface tension force of the water-air interface and the value was taken as 72.8×10^{-3} N/m at 20 °C.

$$\theta_{\mathrm{Adv}} = \cos^{-1}\left(\cos\theta_{\mathrm{Adv},0} + \frac{A\omega^2}{\gamma_{lv}}\right), \tag{23}$$

$$\theta_{\mathrm{Rec}} = \cos^{-1}\left(\cos\theta_{\mathrm{Rec},0} - \frac{A\omega^2}{\gamma_{lv}}\right). \tag{24}$$

The results for CAH are presented in Fig. 6(b) for the horizontal vibration level ($A\omega^2$) changing in the range from 10^{-6} N/m to 5×10^{-4} N/m. It is seen from the graph that at a small vibration level ($A\omega^2 \approx 0$ N/m) the CAH is almost equal to the actual value. Then with the increase of the vibration level, the CAH was reduced dramatically. The CAH hit the minimum value for all three substrates at $A\omega^2 = 5 \times 10^{-4}$ N/m which was considered as the maximum vibration level in this study. Droplets that spontaneously reverse their direction of spreading on special surfaces have been already reported in the literature [31,32].

V. MICROPARTICLE EXTRACTION FROM FLUID FLOW

In the preceding sections, we have discussed several situations in which small-amplitude fast vibrations can be substituted by effective forces. Vibrations of a pipe can also be used for the separation of the multiphase flow consisting, for example, of water and microscale particles like bacteria. This is a typical situation with piezo tube resonators, which are small tubes covered by a piezoelectric material, which provides high-frequency vibrations in the radial direction when liquid flows through the tube. In this section, we model the vibration of the fluid in a tube's cross section by the vibration of an elastic membrane exhibiting specific mode shapes. The microparticles present in the fluid flow are directed towards the nodal locations (nodal circles and lines) of these mode shapes. This effective force driving the microparticles towards the nodal locations can be calculated by applying the separation of motions method.

This theory of effective force derived from small, fast vibration can be applied to the separation of microscale particles, including bacteria, from the fluid flow in a vibrating pipe. Piezo tube resonators consisting of a small metallic tube covered by cylindrical piezoceramics are often used for this purpose. Piezo tubes can be excited at natural frequencies using radial oscillations produced from piezoelectric actuation [33]. The derivation of the effective force corresponding to various modes of vibration is presented in the Supplemental Material [34].

The modulation of electric signal results in small-amplitude fast vibrations of the resonators in the radial direction while liquid columns fill the tubes. Standing cylindrical wave-based mechanisms

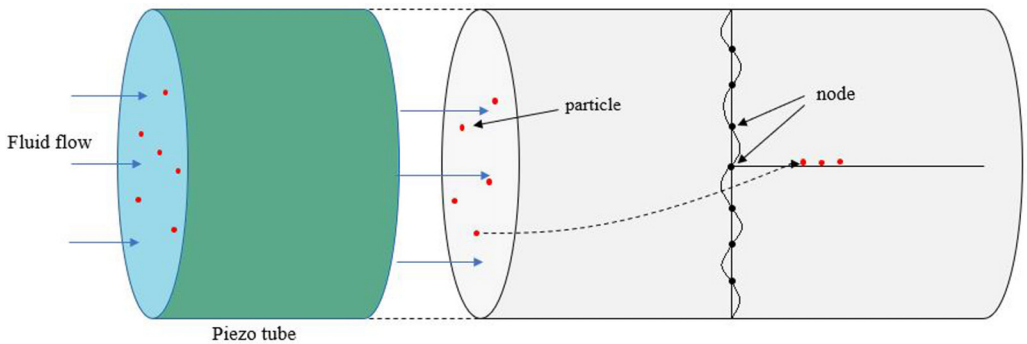

FIG. 7. Fluid passing through a piezo tube resonator where due to small-amplitude fast vibration, microscale particles are concentrated at the central node.

of separating microparticles have been discussed in several studies [35,36]. In our study, we have theorized the microparticle separation using the effective force resulting from small, fast vibration.

When the piezoelectric actuation is applied, the mode shapes on the liquid layers are induced which is analogous to a vibrating membrane. The effective force derived in Eq. (31) drives the microparticles of the multiphase flow to certain controlled locations aligned to the nodal circles and lines corresponding to the frequency of the applied vibration. Depending upon the application and microparticle extraction arrangement used, the convenient frequency for a particular mode shape can be chosen. Then using different microparticle extraction techniques, the particles, such as contaminants or bacteria, can be separated from the flowing fluid.

The calculation of the effective forces on the microparticles (i.e., bacteria) for different vibrational modes for the piezo tube resonator vibration is presented in Eq. (S9) of the Supplemental Material [34]. For a piezo tube of radius $r = 7.5\,\text{mm}$, vibrating at 350 kHz frequency [37] and amplitude $A_{0,2} = 0.001$, the effective force on a bacterium of mass $m = 10^{-15}$ kg is estimated as

$$\begin{aligned} F_{0,2} &= -\tfrac{1}{2}\left(mA_{0,2}^2\right)^2 J_1(5.52) = -\tfrac{1}{2}(10^{-15})(10^{-6})[2\pi(350\times 10^3)]^2 0.340\,27 \\ &= -8.23\times 10^{-10}\ \text{N}. \end{aligned}$$

A schematic diagram of the process of separating microparticles is shown in Fig. 7 where small-amplitude fast vibration is produced using a piezo tube resonator. The piezo tube resonator is vibrated at different frequencies between 50 and 1000 kHz [37].

From the table, it is observed that with the increase of the resonator frequency, the effective force on the bacterium increases accordingly. For the small bacteria, the force is significant enough to drive them to the desired nodal locations.

The experimental study of the suspension separation into fractions under the influence of the standing ultrasonic wave was conducted by Ostasevicius *et al.* [37]. They investigated a suspension of microparticles subject to vibration with the frequency in the range of hundreds of kHz in a piezoelectric cylinder. The observed parameter was the separation time, which was found smaller (4 s) for a water-based suspension than for a biological suspension in a viscous fluid (8 s). Since the velocity scales as the force divided by viscosity, this is consistent with the assumption that the effective force is generated by the vibration.

In a different experimental study, Devendran *et al.* [38] investigated separation of particles of different sizes (10 and 1 μm) in a 1-mm-wide channel subject to the 1.75 MHz frequency. They found that a mode shape with a single node at the center of the channel formed resulting in large particles collected at the nodes of the pressure field, while small particles (whose mass was three orders of magnitude smaller than that of the large particles) followed the streaming patterns, which is in agreement with the theoretical prediction that the effective force depends on the mass.

VI. CONCLUSIONS

We discussed macroscale vibration-induced liquid propulsion effects, such as vibrational jamming of a hole in a water tank on a vibrating foundation and air bubble suction (with the potential for vibrational aeration). These effects have been studied using the mathematical technique called the method of separation of fast and slow motions. The underlying physical reason for these effects is the fundamental asymmetry of the flow in two directions leading to hysteresis. The hysteresis can be utilized by fast small-amplitude vibrations. These are macroscale effects; however, similar effects are also found at the micron scale including vibration-induced superhydrophobicity and phase flow separation. This is because the wetting-dewetting asymmetry is found at the microscale in the form of contact angle hysteresis and adhesion hysteresis. These effects have potential for an application in microfluidics, where capillary forces dominate over viscosity and inertia, in particular, to problems of multiphase flow separation.

ACKNOWLEDGMENT

University of Wisconsin-Milwaukee Research Growth Initiative Grant No. 101X376 is acknowledged.

[1] T. M. Squires and S. R. Quake, Microfluidics: Fluid physics at the nanoliter scale, Rev. Mod. Phys. **77**, 977 (2005).

[2] S. F. Toosi, S. Moradi, and S. Hatzikiriakos, Fabrication of micro/nano patterns on polymeric substrates using laser ablation methods to control wettability behaviour: A critical review, Rev. Adhes Adhes. **5**, 55 (2017).

[3] R. Tadmor, R. Das, S. Gulec, J. Liu, H. E. N'guessan, M. Shah, P. S. Wasnik, and S. B. Yadav, Solid–liquid work of adhesion, Langmuir **33**, 3594 (2017).

[4] J. F. Joanny and P. G. De Gennes, A model for contact angle hysteresis, J. Chem. Phys. **81**, 552 (1984).

[5] S. Srinivasan, G. H. McKinley, and R. E. Cohen, Assessing the accuracy of contact angle measurements for sessile drops on liquid-repellent surfaces, Langmuir **27**, 13582 (2011).

[6] K. J. Kubiak, M. C. T. Wilson, T. G. Mathia, and Ph. Carval, Wettability versus roughness of engineering surfaces, Wear **271**, 523 (2011).

[7] M. Nosonovsky, Multiscale roughness and stability of superhydrophobic biomimetic interfaces, Langmuir **23**, 3157 (2007).

[8] H. Ji, G. Chen, J. Hu, X. Yang, C. Min, and Y. Zhao, Fabrication of a stable superhydrophobic polypropylene surface by utilizing acetone as a non-solvent, J. Dispersion Sci. Technol. **34**, 134 (2013).

[9] S. Lanka, E. Alexandrova, M. Kozhukhova, M. S. Hasan, M. Nosonovsky, and K. Sobolev, Tribological and wetting properties of TiO_2 based hydrophobic coatings for ceramics, ASME. J. Tribol. **141**, 101301 (2019).

[10] G. R. Franzini, A. C. L. Fujarra, J. R. Meneghini, I. Korkischko, and R. Franciss, Experimental investigation of vortex-induced vibration on rigid, smooth and inclined cylinders, J. Fluids Struct. **25**, 742 (2009).

[11] X. Liu, C. Lu, S. Liang, A. Godbole, and Y. Chen, Vibration-induced aerodynamic loads on large horizontal axis wind turbine blades, Appl. Energy **185**, 1109 (2017).

[12] R. A. Stein and M. W. Tobriner, Vibration of pipes containing flowing fluids, J. Appl. Mech. **37**, 906 (1970).

[13] R. Ramachandran, N. Maani, V. L. Rayz, and M. Nosonovsky, Vibrations and spatial patterns in biomimetic surfaces: Using the shark-skin effect to control blood clotting, Philos. Trans. R. Soc., A **374**, 20160133 (2016).

[14] P. Kapitza, Pendulum with a vibrating suspension, Usp. Fiz. Nauk **44**, 7 (1951).

[15] R. Ramachandran and M. Nosonovsky, Vibro-levitation and inverted pendulum: parametric resonance in vibrating droplets and soft materials, Soft Matter **10**, 4633 (2014).
[16] L. D. Landau and E. M. Lifshitz, *Mechanics* (Pergamon Press, Oxford, UK, 1976), Vol. 1, p. 93.
[17] I. I. Blekhman, *Selected Topics in Vibrational Mechanics* (World Scientific, Singapore, 2004), p. 6.
[18] R. L. Daugherty and J. B. Franzini, *Fluid Mechanics*, 6th ed. (New York, McGraw-Hill, 1965), p. 338.
[19] I. I. Blekhman, L. I. Blekhman, L. A. Vaisberg, V. B. Vasil'kov, and K. S. Yakimova, Nonlinear effects observed in the flow of a fluid out of vibrating vessels, Dokl. Phys. **48**, 355 (2003).
[20] H. B. Al Ba'Ba'a, T. Elgammal, and R. S. Amano, Correlations of bubble diameter and frequency for air–water system based on orifice diameter and flow rate, J. Fluids Eng. **138**, 114501 (2016).
[21] E. L. Decker and S. Garoff, Using vibrational noise to probe energy barriers producing contact angle hysteresis, Langmuir **12**, 2100 (1996).
[22] O. Manor, Diminution of contact angle hysteresis under the influence of an oscillating force, Langmuir **30**, 6841 (2014).
[23] L. Dong, A. Chaudhury, and M. K. Chaudhury, Lateral vibration of a water drop and its motion on a vibrating surface, Eur. Phys. J. E **21**, 231 (2006).
[24] X. Noblin, R. Kofman, and F. Celestini, Ratchetlike Motion of a Shaken Drop, Phys. Rev. Lett. **102**, 194504 (2009).
[25] S. Mettu and M. K. Chaudhury, Motion of liquid drops on surfaces induced by asymmetric vibration: Role of contact angle hysteresis, Langmuir **27**, 10327 (2011).
[26] K. X. Yao and H. C. Zeng, Fabrication and surface properties of composite films of SAM/Pt/ZnO/SiO_2, Langmuir **24**, 14234 (2008).
[27] M. E. Schrader, Young-Dupre revisited, Langmuir **11**, 3585 (1995).
[28] M. Nosonovsky and R. Ramachandran, Geometric interpretation of surface tension equilibrium in superhydrophobic systems, Entropy **17**, 4684 (2015).
[29] E. Y. Bormashenko, *Wetting of Real Surfaces* (Walter De Gruyter, Berlin, 2013).
[30] E. B. Dussan and R. T. P. Chow, On the ability of drops or bubbles to stick to non-horizontal surfaces of solids, J. Fluid Mech. **137**, 1 (1983).
[31] S. Tang, Y. Bhimavarapu, S. Gulec, R. Das, J. Liu, H. E. N'guessan, T. Whitehead, C. Yao, and R. Tadmor, Droplets sliding down a vertical surface under increasing horizontal forces, Langmuir **35**, 8191 (2019).
[32] R. Tadmor, A. Baksi, S. Gulec, S. Jadhav, H. E. N'guessan, K. Sen, V. Somasi, M. Tadmor, P. Wasnik, and S. Yadav, Drops that change their mind: Spontaneous reversal from spreading to retraction, Langmuir **35**, 15734 (2019).
[33] N. H. Asmar, *Partial Differential Equations with Fourier Series and Boundary Value Problems*, 2nd ed. (Pearson Prentice Hall, NJ, 2004), p. 207–252.
[34] See Supplemental Material at http://link.aps.org/supplemental/10.1103/PhysRevFluids.5.054201 for mathematical derivations.
[35] D. Bavli, Y. Barenholz, N. Emanuel, V. Ponomarev, and A. Priev, Ultrasound-enhanced latex immunoassay of pathogens in water, J. Acoust. Soc. Am. **123**, 3789 (2008).
[36] A. Priev and A. Sarvazyan, Cylindrical standing wave resonator for liquid food quality control, J. Acoust. Soc. Am. **125**, 2593 (2009).
[37] V. Ostasevicius, V. Jurenas, I. Golinka, R. Gaidys, and A. Aleksa, Separation of microparticles from suspension utilizing ultrasonic standing waves in a piezoelectric cylinder actuator, Actuators **7**, 14 (2018).
[38] C. Devendran, I. Gralinski, and A. Neild, Separation of particles using acoustic streaming and radiation forces in an open microfluidic channel, Microfluid. Nanofluid. **17**, 879 (2014).

Correction: The works cited as Refs. [19] and [20] have been interchanged and some citations in text have been adjusted. Minor errors in Eqs. (18), (19), and (21)–(24) have also been rectified.